Electrophoretically Deposited Layers of Octahedral Molybdenum Cluster Complexes: A Promising Coating for Mitigation of Pathogenic Bacterial Biofilms under Blue Light

Kaplan Kirakci, Thi Kim Ngan Nguyen, Fabien Grasset, Tetsuo Uchikoshi, Jaroslav Zelenka, Pavel Kubát, Tomáš Ruml, Kamil Lang

HAL Id: hal-03052917

https://univ-rennes.hal.science/hal-03052917

Submitted on 12 Feb 2021

Electrophoretically Deposited Layers of Octahedral Molybdenum Cluster Complexes: A Promising Coating for Mitigation of Pathogenic Bacterial Biofilms under Blue Light

Journal:	*ACS Applied Materials & Interfaces*
Manuscript ID	am-2020-190365.R1
Manuscript Type:	Article
Date Submitted by the Author:	04-Nov-2020
Complete List of Authors:	KIRAKCI, Kaplan; Akademie Ved Ceske Republiky Ustav anorganicke chemie, NGUYEN, Thi Kim Ngan; National Institute for Materials Science, Fine Particle Engineering Grasset, Fabien; CNRS, UMI3629 UCHIKOSHI, Tetsuo; National Institute for Materials Science, Research Center for Functional Materials Zelenka, Jaroslav; Vysoka skola chemicko-technologicka v Praze, Dpt. of Biochemistry and Microbiology Kubát, Pavel; J Heyrovsky Institute of Physical Chemistry Czech Academy of Sciences, Spectroscopy Ruml, Tomáš; Vysoka skola chemicko-technologicka v Praze, Dpt. of Biochemistry and Microbiology Lang, Kamil; Institute of Inorganic Chemistry of the Czech Academy of Sciences,

SCHOLARONE™
Manuscripts

Electrophoretically Deposited Layers of Octahedral Molybdenum Cluster Complexes: A Promising Coating for Mitigation of Pathogenic Bacterial Biofilms under Blue Light

Kaplan Kirakci,[a],* Thi Kim Ngan Nguyen,[b,c] Fabien Grasset,[b,c] Tetsuo Uchikoshi,[b,c] Jaroslav Zelenka,[d] Pavel Kubát,[e] Tomáš Ruml,[d] Kamil Lang [a],*

[a] Institute of Inorganic Chemistry of the Czech Academy of Sciences, Řež 1001, 250 68 Husinec-Řež, Czech Republic

[b] CNRS – Saint-Gobain – NIMS, UMI 3629, Laboratory for Innovative Key Materials and Structures (LINK), National Institute for Materials Science, 1-1 Namiki, 305-0044 Tsukuba, Japan

[c] Research Center for Functional Materials, National Institute for Materials Science (NIMS), 1-2-1 Sengen, Tsukuba, Ibaraki 305-0047, Japan

[d] Department of Biochemistry and Microbiology, University of Chemistry and Technology Prague, Technická 5, 166 28 Praha 6, Czech Republic

1

[e] J. Heyrovský Institute of Physical Chemistry of the Czech Academy of Sciences, Dolejškova 3,

182 23 Praha 8, Czech Republic

ABSTRACT

The fight against infective microorganisms is becoming a worldwide priority due to serious

concerns about the rising numbers of drug-resistant pathogenic bacteria. In this context, the

inactivation of pathogens by singlet oxygen, $O_2(^1\Delta_g)$, produced by photosensitizers upon light

irradiation has become an attractive strategy to combat drug-resistant microbes. To achieve this

goal, we electrophoretically deposited $O_2(^1\Delta_g)$-photosensitizing octahedral molybdenum cluster

complexes on indium-tin oxide coated glass plates. This procedure led to the first example of

molecular photosensitizer layers able to photoinactivate bacterial biofilms. We delineated the

morphology, composition, luminescence, and singlet oxygen formation of these layers and

correlated these features with their antibacterial activity. Clearly, continuous 460 nm light

irradiation imparted the layers with strong antibacterial properties, and the activity of these layers

inhibited the biofilm formation and eradicated mature biofilms of Gram-positive *Staphylococcus

aureus* and *Enterococcus faecalis*, as well as, Gram-negative *Pseudomonas aeruginosa* and

Escherichia coli bacterial strains. Overall, the microstructure-related oxygen diffusivity of the

layers and the water stability of the complexes were the most critical parameters for the efficient

and durable use. These photoactive layers are attractive for the design of antibacterial surfaces

activated by visible light and include additional functionalities such as the conversion of harmful UV/blue light to red light or oxygen sensing.

1. INTRODUCTION

The octahedral molybdenum cluster complexes (Mo_6) have recently come forth as potent red luminophores and singlet oxygen photosensitizers readily excitable *via* UV and visible light up to 550 nm, and even by X-ray irradiation.[1,2,3,4,5] These complexes generally denoted $[Mo_6L^i_8L^a_6]^n$ (L^a = halogen inner ligand, L^i = inorganic or organic apical ligands, $-2 \leq n \leq 4$) form long-lived excited triplet states that relax *via* red luminescence with high quantum yields and are efficiently quenched by molecular oxygen producing singlet oxygen, $O_2(^1\Delta_g)$, in high yields.[1,2,3,4] It is worth mentioning that, in contrast with a typical organic photosensitizer such as porphyrins, singlet oxygen is produced by Mo_6 cluster complexes even in the solid state allowing for the preparation of photosensitizing materials with a high concentration of active cluster complexes.[5] This sensitization ability has been exploited for the design of various functional materials for photodegradation of pollutants,[6] photo/radiosensitized killing of tumor cells,[5,7,8,9,10,11,12] or photodynamic inactivation of bacteria.[13,14,15,16] The high efficacy of this modality in photoinactivation of bacteria stems from the fact that $O_2(^1\Delta_g)$ attacks several critical targets of pathogens, thus making their resistance unlikely.

Only several studies have concentrated on the development of antibacterial materials composed of singlet oxygen-producing Mo_6 complexes so far. Galindo *et al.* described the bacterial photoinactivation properties of Mo_6 complexes immobilized in polystyrene gel.[13,14] Shestopalov *et al.* investigated the antibacterial activity of fluorinated polymer films immobilized cluster complexes.[15,17] Our group recently reported the photoinactivation properties

of a positively charged Mo_6 complex.[16] However, the more challenging, not yet achieved with Mo_6 complexes, is the photodynamic inactivation of microbial biofilms. A biofilm is a natural form of microbial existence on surfaces including medical equipment, food packaging, or industrial facilities. It is often well structured, multispecies, metabolically symbiotic, and communicating society, containing a significant amount of an extracellular scaffold. Microbial biofilms tend to be several orders of magnitude more resistant to antibiotics, disinfection, and desiccation than separated microbes.[18]

In parallel, the electrophoretic deposition (EPD) became, very recently, one of the successful strategies for fabricating nanostructured layers composed of transition metal octahedral clusters.[19,20,21] The EPD occurs at room temperature and allows for controlling the layer thickness within a short time. The octahedral structure of the cluster core as well as the optical properties are preserved while applying an electric field and, thus, the EPD was utilized for preparing thin and transparent nanocomposite layers with properties well suited for optical and energy applications.[22,23,24,25]

Herein, we utilized the EPD of dissolved $Na_2[Mo_6I_8(OPOPh_2)_6]$ (**1**) and $[Mo_6I_8(OCOC_4H_8PPh_3)_6]Br_4$ (**2**) compounds on indium-tin oxide (ITO) coated glass plates to prepare the layers whose function is triggered by visible light (Figure 1). The structural and photochemical properties of the layers together with their enhanced antibacterial activity against Gram-positive and Gram-negative bacterial biofilms make the EPD one of the highly efficient techniques for the fabrication of transparent antibacterial coatings.
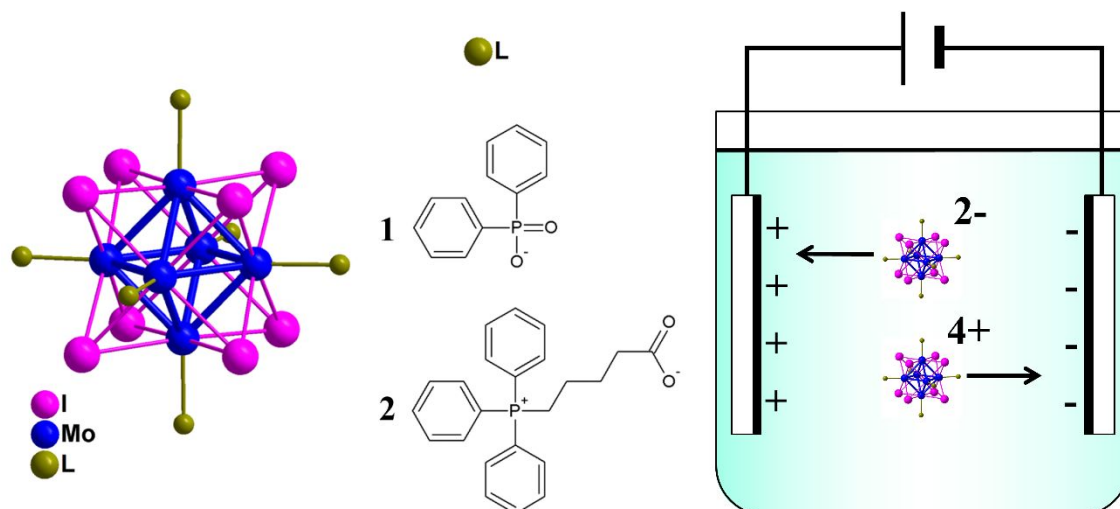
Figure 1. Schematic representation of complexes $[Mo_6I_8(OPOPh_2)_6]^{2-}$ (**1**) and $[Mo_6I_8(OCOC_4H_8PPh_3)_6]^{4+}$ (**2**) and their electrophoretic deposition on ITO glass plates.

2. EXPERIMENTAL SECTION

2.1. Reagents and General Procedures. Compounds $Na_2[Mo_6I_8(OPOPh_2)_6]$ (**1**) and $[Mo_6I_8(OCOC_4H_8PPh_3)_6]Br_4$ (**2**) were prepared according to previously published procedures.[12,16] The EPD system includes two ITO coated glass plates (6.15-7.27 Ohm/sq, Geomatec Co., Ltd. Tokyo, Japan), acting as electrodes which are connected to a Source Meter (Keithley Model 2400, Ohio, USA). The ITO plates, with a surface area of 1.0×2.0 cm^2, were contacted with electrodes bar by using a conductive aluminum double side tape. The molecules of Mo_6 complexes are set in motion by applied current and deposit on ITO coated glass plates to form thin layers (Figure 1).

2.2. Instrumental Techniques. The surface morphology and cross-section of Mo_6 layers were analyzed using a field emission scanning electron spectroscope (FE-SEM, Hitachi S4800) operated at 10 kV. The diffraction patterns of the layers were identified by X-ray diffraction

analyses (XRD) (Altima 3, Rint 2000, Rigaku Corp.), operated at 40 kV and 30 mA in the 2θ

angle range with Cu Kα radiation (λ = 0.15405 nm). X-ray photoelectron spectroscopy (XPS) of

the deposited layers was performed with a PHI Quantera SXM (ULVAC-PHI) using Al Kα

radiation at 20 kV and 5 mA, neutralization by Ar^+, and a take-off angle of 45°. All binding

energies were calibrated with respect to the C 1s peak of adventitious carbon at 285 eV.

Luminescence was monitored on a Fluorolog 3 spectrometer equipped with a cooled TBX-05-

C photon detection module (Horiba Jobin Yvon) or a Hamamatsu H10330-45 photomultiplier in

air. The latter set-up was used for the detection of the singlet oxygen formation. Absolute

photoluminescence quantum yields were measured using a Quantaurus QY C11347-1

spectrometer (Hamamatsu) in air with a neat ITO plate as a blank (400 nm excitation). Time-

resolved luminescence at 700 nm was measured using an LKS 20 laser kinetic spectrometer

(Applied Photophysics, UK) equipped with a Hamamatsu R928 photomultiplier. The layer was

inserted into a quartz cell and evacuated at least 15 min by a rotary pump for measurements in a

vacuum. Then, selected oxygen pressures were applied. The layers were excited with a Quantel

Q Smart 450 Nd YAG laser (excitation wavelength of 355 nm, fwhm ~5 ns). The kinetic traces

were fitted to a double exponential function. The amplitude average luminescence lifetime (τ) at

given oxygen pressure (p_{O2}) was calculated as $\tau = (A_1\tau_1 + A_2\tau_2)/(A_1+A_2)$, where A_i and τ_i are the

amplitudes and lifetimes of individual processes, respectively. The rate constant for

luminescence quenching by oxygen (k_q) was obtained from the slope of the Stern-Volmer plot

$1/\tau = 1/\tau_0 + k_q\, p_{O2}$, where τ_0 is the corresponding luminescence lifetime in a vacuum.

2.3. Preparation of 1/ITO Glass. Compound **1** was dissolved in acetone (99.5 %, Nacalai

Tesque, Inc.) at a concentration of 5 g L^{-1} by using ultra-sonication for 10 min. The layers were

prepared by the anodic EPD at 50 V for 30 s. XPS (in molar ratios): Mo/I/P/Na: calcd. 6.0/8.0/6.0/2.0; found 6.0/8.2/6.0/2.0.

2.4. Preparation of 2/ITO Glass. Compound **2** was dissolved in the mixed solvent of methyl ethyl ketone (99 %, Nacalai Tesque, Inc.) and methanol (99,8 %, Nacalai Tesque, Inc.) at a concentration of 1g L^{-1} by using ultra-sonication for 30 min. The volume ratio of methyl ethyl ketone/methanol was 83.3. The layers were prepared by the cathodic EPD process at 10 V for 30 seconds. XPS (in molar ratios): Mo/I/P/Br: calcd. 6.0 /8.0/6.0/4.0; found 6.0 /7.8/4.0/2.3.

2.5. Biological Testing. The bacterial strains of *Escherichia coli*, *Pseudomonas aeruginosa*, *Staphylococcus aureus*, and *Enterococcus faecalis* were obtained from the Collection of Yeasts and Industrial Microorganisms of the University of Chemistry and Technology Prague. The strains were cultivated on Luria-Bertani (LB) agar plates and stored at 4 °C for up to one month. The inoculum was prepared 24 hours before the experiment in the fresh LB medium. The bacterial concentration was 1 McFarland = 3×10^6 cells mL^{-1}. During the inhibition experiments, an ITO coated glass plate was immersed vertically into the fresh medium with 10% of the inoculum and incubated for the indicated time with or without irradiation with a 460 nm LED light source. For the experiments with biofilm eradication, the bacterial biofilm was allowed to form on a plate for 24 hours before irradiation. After irradiation, the plate was gently washed three times with phosphate-buffered saline (PBS) and immersed into fresh PBS in a clean vial. The vial was subjected to ultrasound in a water bath set to 50 W for 5 minutes. The resuspended bacteria were vortexed, serially diluted with PBS, and spread onto LB agar plates. After 24h incubation at 37 °C, the colony-forming units (CFU) were counted. The integrity of the biofilm during the procedure was continuously monitored with an inverted microscope. The absolute densities of untreated biofilms under standard conditions in CFU were not dependent on the type

of the layer and were in average as follow: *E. coli* 1×10^7 cm^{-2}, *S. aureus* 7×10^7 cm^{-2}, *E. faecalis* 6×10^6 cm^{-2}, *P. aeruginosa* 2×10^7 cm^{-2}.

3. RESULTS AND DISCUSSION

3.1. Characterization of the EPD layers. The EPD method was applied to fabricate layers composed of Mo_6 complexes on ITO coated glass plates. The compounds selected for deposition were: $Na_2[Mo_6I_8(OPOPh_2)_6]$ (**1**) with unmatched stability against hydrolysis and high quantum yield of the singlet oxygen formation,[12] and $[Mo_6I_8(OCOC_4H_8PPh_3)_6]Br_4$ (**2**) which constitutes a rare example of positively charged Mo_6 complex with the ability to photoinactivate Gram-positive bacteria.[16] Due to the different charges of the two complexes, **1** and **2** were deposited *via* the anodic and cathodic EPD arrangement, respectively. The deposition conditions (solvent, concentration, voltage, and deposition time) were optimized in order to reach the highest thickness of the deposited layers, while maintaining the neat appearance of the layers. This led in both cases to yellow transparent layers as visualized in Figure 2. Scanning electron microscopy revealed that the **1/ITO glass** layer was approximately 1200 nm thick and showed a rough surface caused by condensation of approximately 200 nm particles of **1** (Figure 2a, Figure S1). The **2/ITO glass** layer had approximately 700 nm thickness and was characterized by a flat and homogeneous surface area sprinkled by a small number of aggregates of **2** (Figure 2b, Figure S1).
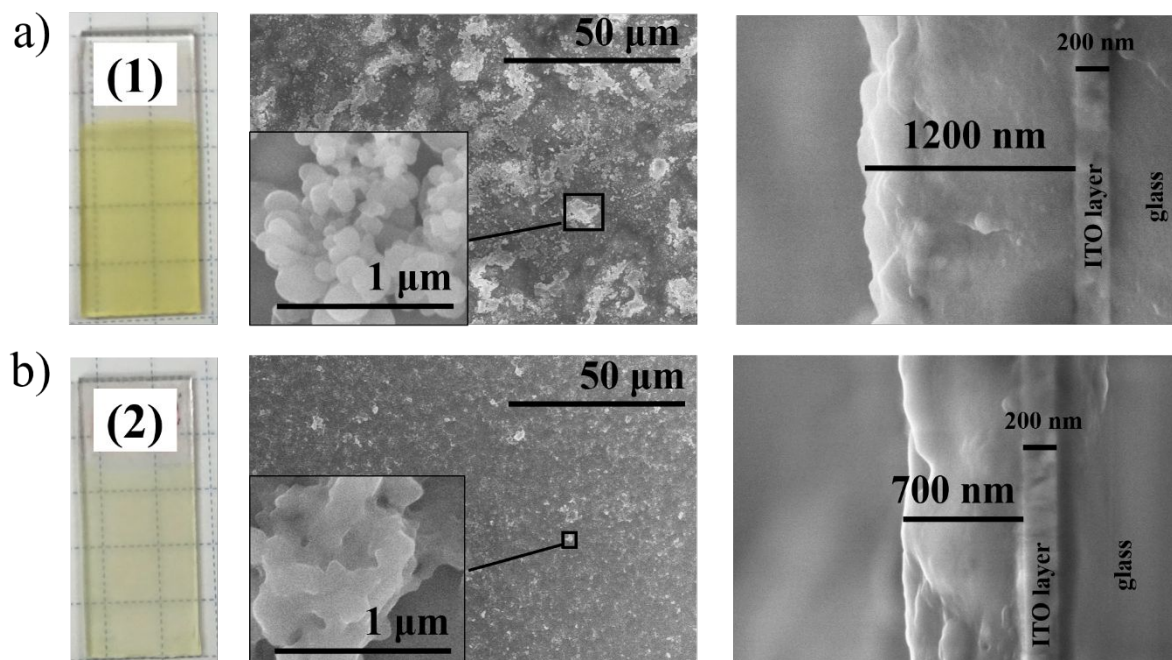
Figure 2. Photographs of the **1/ITO glass** (a) and **2/ITO glass** (b) layers under visible light (left), surface morphology (middle), and cross-section (right) images**.**

XPS-based quantitative elemental analysis of the **1/ITO glass** layer confirmed the superior stability of the complex as it remained intact during the deposition process with no sign of hydrolysis of the diphenylphosphinate apical ligands as evidenced by a P : Mo ratio of 6.0 : 6.0 (Figure S2). This observation differs considerably from the general behavior of anionic Mo_6 complexes, which were reported to hydrolyze during the EPD deposition.[19] In addition, a molar ratio Na : Mo of 2.0 : 6.0 indicated that two sodium cations compensate for the complex dianion within the layer and that the composition of the deposited layer is $Na_2[Mo_6I_8(OPOPh_2)_6]$, i.e., the same as the composition of original compound **1**. This behavior contrasts with previous findings showing that anionic Mo_6 complexes were neutralized by hydronium H_3O^+, generated on the anode by protolysis of H_2O.[19,20] On the other hand, compound **2** hydrolyzed during the EPD as indicated by a measured deficit of two triphenylphosphonium ligands (molar ratio P : Mo was

only 4.0 : 6.0) and overall dicationic charge compensated by two bromide anions (molar ratio Br

: Mo was approximately only 2.3 : 6.0) (Figure S3). Based on these results, the composition of

the **2/ITO glass** layer can be approximated by the formula of $[Mo_6I_8(OCOC_4H_8PPh_3)_4(OH)_2]Br_2$.

Figure S4 presents the XRD patterns of the **1/ITO glass** and **2/ITO glass** layers. Both samples

showed the peaks assigned to the ITO layer. The **1/ITO glass** sample showed an additional broad

peak appearing at 7º (2θ), which is generally assigned to ill ordered Mo_6 complexes.[18,20] A

similar diffraction peak, however, of much lower intensity, was also observed for **2/ITO glass**.

The lower intensity is probably due to a smaller thickness of the layer, when compared with

1/ITO glass, and to the amorphous character of the partially hydrolyzed layer.

Absorption spectra of the layers were typical for Mo_6 complexes with a broad band between

350 and 450 nm and an onset at approximately 550 nm (Figure 3A). Thus, the deposited layers

were well transparent in the visible region and blocked UVA radiation below 350 nm

considerably. Both layers displayed broad luminescence bands with maxima at 695 nm and 706

nm, respectively (Figure 3B). These bands were blue-shifted when compared to luminescence of

powders of **1** and **2** (702 and 724 nm, respectively), due to the different local environment of the

complexes between the layers and the microcrystalline powders (Figure S5). The use of such

layers for photoinactivation of biofilms requires long-term stability in an environment of high

moisture. This can be critical for Mo_6 complexes which are often susceptible to hydrolysis. To

simulate such an environment, the layers were soaked in deionized water for one week, dried in

the air atmosphere, and their luminescence spectra were measured afterward (Figure S6). The

results documented that the **1/ITO glass** layers have unchanged luminescence spectra, which

confirm the stability of the layers made of **1** in a water environment.[12] On the other hand, the

luminescence band of the **2/ITO glass** layers underwent a red shift to 715 nm with a

considerable decrease of the luminescence quantum yield, which is indicative of further hydrolysis of **2** in the layer.

The luminescence quantum yields were 0.06 and 0.11 for **1/ITO glass** and **2/ITO glass** in air, respectively, and were significantly lower than those of pure **1** and **2** (0.24 and 0.34, respectively) (Table 1). The lower luminescence quantum yield of **1/ITO glass**, when compared with **1**, suggested efficient quenching of **1** in **1/ITO glass** in air, i.e., much better accessibility of the triplet states of deposited **1** to molecular oxygen than in the corresponding powder. To unravel the mechanism behind the discrepancy between the photophysical properties, the decay luminescence kinetics of **1** and **1/ITO glass** were investigated at different oxygen pressures (Figure 3, Figure S7). In the case of **1/ITO glass**, the Stern-Volmer plot was linear and the adequate quenching rate constant was 95 s^{-1} $Torr^{-1}$. Thus, this layer is also suited for the luminescence measurement of local oxygen concentrations.[26] On the contrary, the Stern-Volmer plot for the powder of **1** displayed downward curvature suggesting that a considerable amount of the triplet states is inaccessible to molecular oxygen. Indeed, the quenching rate constant was reaching approximately 82 s^{-1} $Torr^{-1}$ only at low oxygen pressures due to quenching of the surface-located triplet states by oxygen. At higher oxygen pressures, the luminescence intensity of the accessible fraction was quenched, whereas the buried, inaccessible fraction remained unaffected. These results documented that the triplet states of **1** arranged in approximately 200 nm particles within the layer (Figure 2a) are accessible to molecular oxygen and can generate $O_2(^1\Delta_g)$ within the layer volume.

The oxygen quenching was one order of magnitude less effective for **2/ITO glass**. The quenching rate constant was approximately 10 s^{-1} $Torr^{-1}$, suggesting a much slower diffusion motion of oxygen in **2/ITO glass** than in **1/ITO glass** (Figure 3, Figure S7). The powder of **2**

behaved in the same way with a quenching rate constant of approximately 7 s^{-1} Torr^{-1} (Figure S7). Clearly, low diffusivity of oxygen originates from intermolecular or microstructural effects within the microcrystalline powder of **2** or the solid layer of partially hydrolyzed **2** in **2/ITO glass** (Figure 2b), as solutions of **2** were shown to display efficient quenching of luminescence by oxygen.[16] Since the accessibility of the triplet states to oxygen is similar in **2** and **2/ITO glass**, the lower luminescence quantum yield of **2/ITO glass** compared with **2** is caused by the extensive contribution of competitive nonradiative relaxation of the triplet states within the layer. Such behavior is known to occur upon hydrolysis of Mo$_6$ complexes,[16] which is the case of **2/ITO glass** as documented above.

In both **1/ITO glass** and **2/ITO glass**, luminescence quenching by oxygen indicated the formation of O$_2$($^1\Delta_g$), which was confirmed directly by measuring its typical luminescence band centered at approximately 1270 nm (Figure S8). This work documents advantages of Mo$_6$ complexes over common organic molecules, which are often utilized as photosensitizers of O$_2$($^1\Delta_g$). Many organic photosensitizers are efficient producers of O$_2$($^1\Delta_g$) in solutions, however, once deposited on supporting materials, their packing and aggregation in the solid state have generally detrimental effects on productivity of O$_2$($^1\Delta_g$).[27] In contrast, Mo$_6$ complexes have strong luminescence originating from the triplet states even in the solid state, and when oxygen is present, the triplet states of these complexes are quenched to produce O$_2$($^1\Delta_g$) with a high efficacy.[26] Thus, Mo$_6$-based nanoparticles and composites are effective photosensitizers and can serve for the construction of photoactive materials producing O$_2$($^1\Delta_g$) for oxidation reactions in an easily separable form, antibacterial surfaces, or for optical oxygen sensing in biological systems.

Table 1. Photophysical parameters of **1/ITO glass** and **2/ITO glass** at room temperature.[a]

	λ_L / nm	Φ_L	τ_0/ μs	k_q / s^{-1} $Torr^{-1}$
1	702	0.24±0.01	97	82[b]
1/ITO glass	695	0.06±0.01	36	95
2	724	0.34±0.01	34	7
2/ITO glass	706	0.11±0.01	35	10

[a] λ_L is the maximum of luminescence emission bands (λ_{exc} = 400 nm); Φ_L is the luminescence quantum yields in air (λ_{exc} = 400 nm); τ_0 is the average luminescence lifetime measured in a vacuum (λ_{exc} = 355 nm, λ_{em} = 700 nm); k_q is the rate constant of luminescence quenching by oxygen. [b] Nonlinear Stern-Volmer plot, estimated at low oxygen pressures.
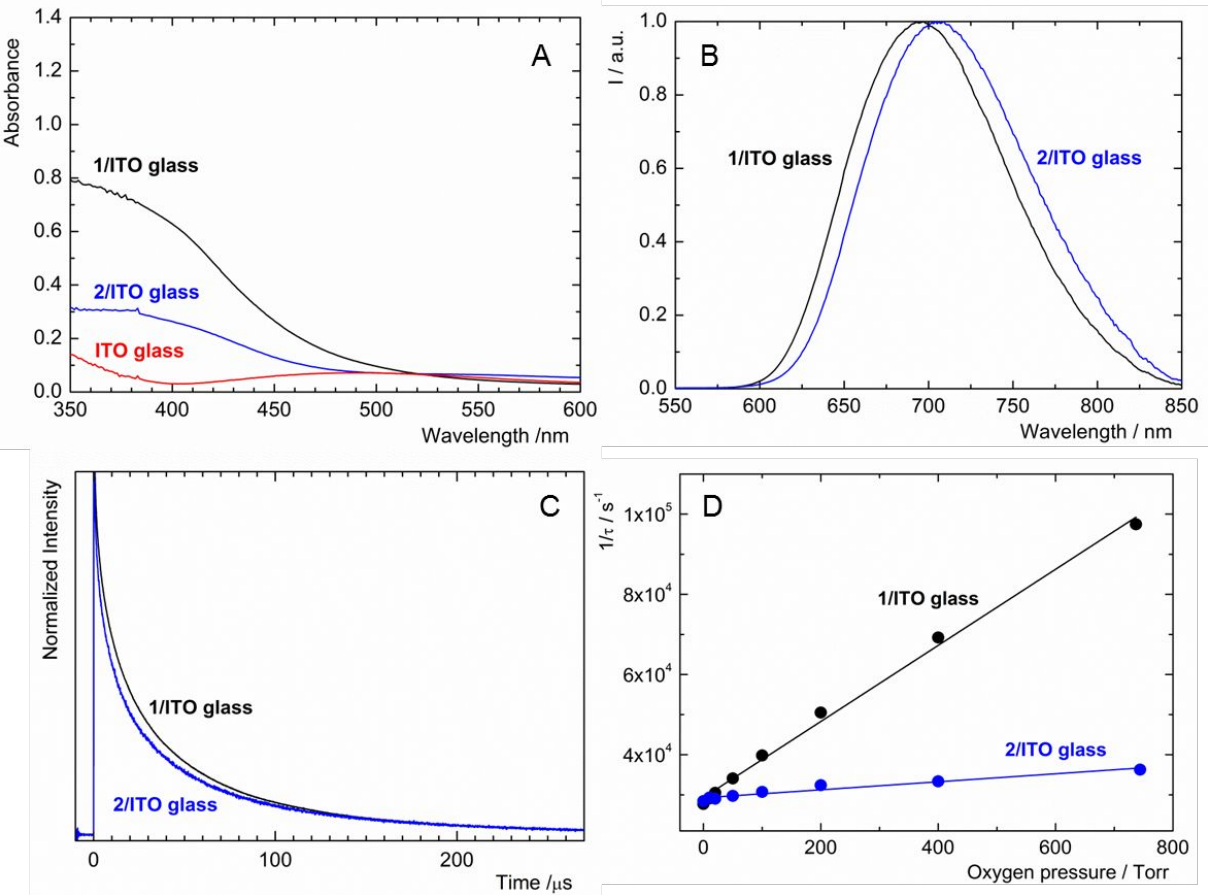
Figure 3. Absorption and luminescence properties of deposited layers of **1** and **2** on ITO glass plates: (A) Absorption spectra. (B) Normalized luminescence emission spectra in air (excited at 400 nm). (C) Time-resolved luminescence of **1/ITO glass** and **2/ITO glass** recorded at 700 nm in a vacuum (excited at 355 nm) and (D) the corresponding Stern-Volmer plots for luminescence quenching by oxygen, where τ is the average luminescence lifetime.

3.2. Inhibition of Biofilm Formation. We performed a set of experiments focused on the inhibition of biofilm formation. The continuous 24h irradiation with 460 nm light (4.5 mW cm^{-2}) of **1/ITO glass** caused a significant decrease in the number of viable biofilm bacteria (Figure 4A). Interestingly, the expected distinctive effect on the Gram-negative and Gram-positive bacteria due to their different cell wall structure was not confirmed. The Gram-positive bacteria exhibited intermediate sensitivity, whilst the two Gram-negative representatives, i.e., *P. aeruginosa* and *E. coli* were the most susceptible and the most resistant strains, respectively. Nevertheless, the parallel experiment with **2/ITO glass** showed a considerable, but less pronounced inhibitory effect with the exact opposite order of the strains susceptibility (Figure 4B). Since the complex in **1/ITO glass** has a net negative charge and in **2/ITO glass** has a net positive charge, these differences in sensitivity may be caused by a different charge of the outer bacterial surface.[28] The Gram-positive strains are more negatively charged due to the presence of phosphates in teichoic acid, which is the dominant component of their cell walls, but it is absent in Gram-negative bacteria. The situation is more complicated in the mature biofilm (see below), where also Gram-negative strains significantly increase their negative charge due to the formation of extracellular polymeric substances including DNA a polysaccharide.[29]

Constrained diffusion of oxygen in the volume of **2/ITO glass** when compared to **1/ITO glass** evidently did not affect the production of cytotoxic $O_2(^1\Delta_g)$ near the surface with adsorbed bacteria. Therefore, both layers even the one with limited oxygen permeability exhibited similar phototoxicity towards *E. coli* and *S. aureus* strains. Importantly, we observed no inhibitory effect upon irradiation of biofilms grown on negative control, i.e., pure ITO glass plates (Figure S9).

The practical application of the anti-biofilm surfaces requires considerable stability of the phototoxic effect, especially to function upon repeated exposure. Therefore, the already once used layers were washed using an ultrasonic bath, dried, and used repeatedly in another 24 h experiment to test their efficiency in repeated inhibition of *E. coli* biofilm formation. The *E. coli* strain was selected as the most resistant strain on **1/ITO glass**. The result of **1/ITO glass** showed a slight decrease in the inhibition efficiency from the 69%-efficiency in the first usage to 56 %-efficiency. In contrast, **2/ITO glass** completely lost the inhibitory effect in the second successive experiment, probably due to further progress of hydrolysis of **2**, resulting in limited singlet oxygen productivity (Figure S10).
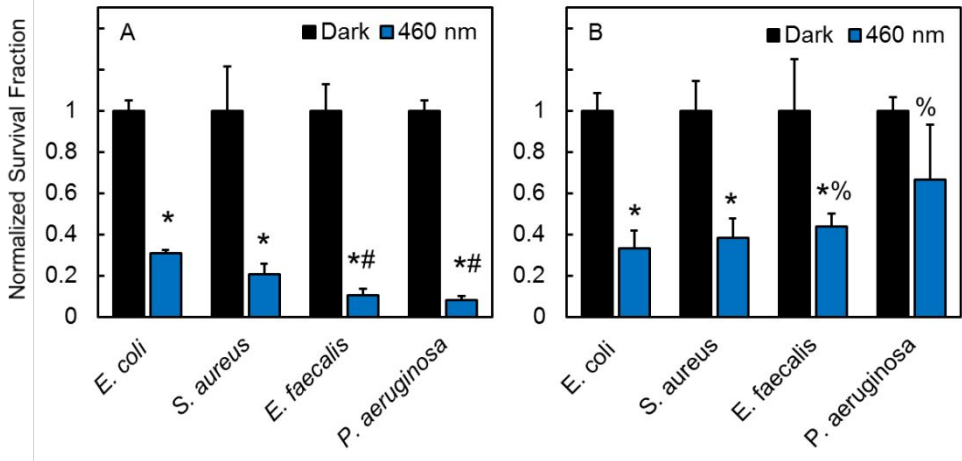

Figure 4. Inhibition of biofilm formation on **1/ITO glass** (A) and **2/ITO glass** (B) after continuous 24h irradiation with 460 nm light (4.5 mW cm^{-2}). Notes: * significantly different

from the respective dark control; # significantly different from *E. coli* under 460 nm light; %

significantly different from the respective result on **1/ITO glass**.

3.3. Eradication of Matured Biofilms. The exposure of well-grown biofilms on **1/ITO glass**

to 460 nm light (18 mW cm^{-2}) for 1 hour resulted in a significant decrease in the number of

viable bacteria in the biofilms (Figure 5A). There was no trend regarding the different structures

of the Gram-positive and Gram-negative cell walls of bacteria. Most responsive strains were

Gram-positive *S. aureus* and Gram-negative *P. aeruginosa*, while Gram-positive *E. faecalis* and

Gram-negative *E. coli* were less sensitive. The discrepancy in susceptibility is probably the

outcome of the different structure of the biofilm matrices. On the contrary, the effect of **2/ITO**

glass under the same conditions was generally much weaker likely in accordance with the lower

diffusivity of oxygen within the cluster layer as the number of $O_2(^1\Delta_g)$ molecules produced at the

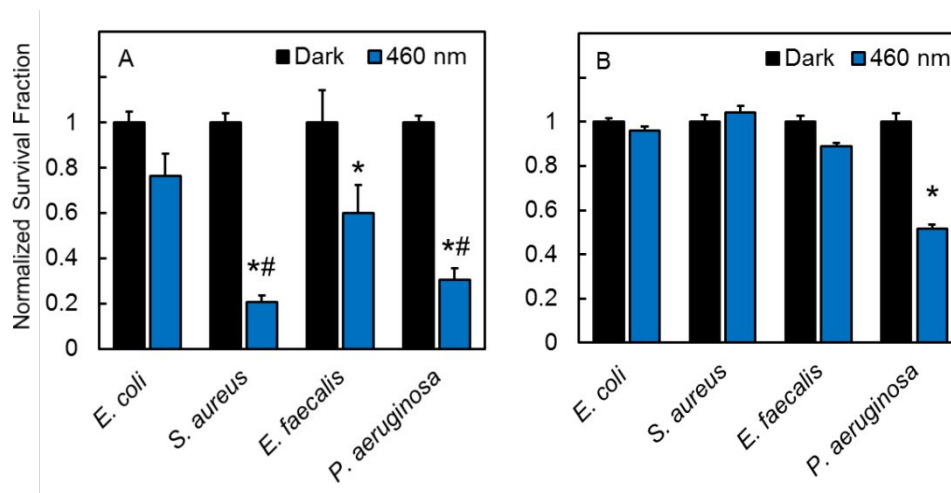surface was not enough to eradicate dense matured biofilms (Figure 5B).

Figure 5. Eradication of matured biofilms on **1/ITO glass** (A) and **2/ITO glass** (B) after

exposure to 460 nm light for 1 h (18 mW cm^{-2}). Notes: * significantly different from the

respective dark control; # significantly different from *E. coli* under 460 nm light.

It is known that the conventional treatment of matured biofilms by antibiotics is ineffective and the development of alternative biofilm-eradiation agents is essential to combat microbial infections.[30,31] Our results demonstrate that **1/ITO glass** displays high photodynamic efficiency, preventing the early stages of biofilm formation and eradicating matured biofilms. The basic mechanism is based on photooxidation by $O_2(^1\Delta_g)$, but some contribution of photothermal processes, as described for several light-triggered antibacterial materials, cannot be excluded.[32] In comparison with semiconductor-based materials for biofilm control that often requires complex architectures,[33,34] the preparation of our materials by the EPD of Mo_6 complexes is straightforward, inexpensive, and promising for the design of self-sterilizing or self-sanitizing surfaces in healthcare, pharmaceutical, and food industry.[35]

4. CONCLUSION

We prepared the first molecular photosensitizer layers for the photodynamic inactivation of biofilms. Materials based on pure layers of common singlet oxygen photosensitizers, such as porphyrins or other organic dyes, are strongly affected by their aggregation resulting in a detrimental effect on the $O_2(^1\Delta_g)$ generation. In this respect, the cluster complexes can generate $O_2(^1\Delta_g)$ even in the solid state, a feature which allows for the fabrication of simple, one-component functional layers.

The prepared layers displayed different behavior in terms of photosensitizing activity rising mainly from their microstructure-related oxygen diffusivity and from the distinct water stability of the complexes used for the EPD. This behavior is translated into a higher biofilm eradication of Gram-positive *S. aureus* and *E. faecalis* as well as Gram-negative *P. aeruginosa* and *E. coli*

bacterial strains under 460 nm irradiation for **1/ITO glass** than for **2/ITO glass**. Nevertheless, both layers displayed strong inhibition of the biofilm growth with a slightly different trend depending on the bacterial type possibly related to the surface charge of the layers. Both Gram-positive and Gram-negative bacteria frequently occur in mixed biofilms involved in numerous infections, and therefore the resulting materials capable to inhibit both types of bacteria are attractive for the development of light-activated antibacterial surfaces for sterilization of medical devices and implants. In addition to biofilm eradication, the layers have more functionalities. They protect from harmful UVA/blue light by converting it to red light, and oxygen-dependent quenching of the Mo_6-based luminescence is a measure of local oxygen concentrations. Thus, these multifunctional layers can be utilized as optical oxygen sensors or UVA/blue-light screen filters.

ASSOCIATED CONTENT

Supporting Information

The Supporting Information is available free of charge at……

SEM images, XPS spectra, luminescence spectra, luminescence decay curves, and Stern-Volmer plots, luminescence emission bands of $O_2(^1\Delta_g)$, control experiments on the neat ITO glass plate, repeated applications of the layers.

AUTHOR INFORMATION

Corresponding Authors

Kamil Lang - Institute of Inorganic Chemistry of the Czech Academy of Sciences, Řež 1001, 250 68 Husinec-Řež, Czech Republic; Email: lang@iic.cas.cz

Kaplan Kirakci - Institute of Inorganic Chemistry of the Czech Academy of Sciences, Řež 1001, 250 68 Husinec-Řež, Czech Republic; Email: kaplan@iic.cas.cz

ACKNOWLEDGMENTS

REFERENCES

1 Maverick, A. W.; Najdzionek, J. S.; MacKenzie, D.; Nocera, D. G.; Gray, H. B. Spectroscopic, Electrochemical, and Photochemical Properties of Molybdenum(II) and Tungsten(II) Halide Clusters. *J. Am. Chem. Soc*. **1983**, *105*, 1878-1882.

2 Kirakci, K.; Kubát, P.; Langmaier, J.; Polívka, T.; Fuciman, M.; Fejfarová, K.; Lang, K. A Comparative Study of the Redox and Excited State Properties of (nBu$_4$N)$_2$[Mo$_6$X$_{14}$] and (nBu$_4$N)$_2$[Mo$_6$X$_8$(CF$_3$COO)$_6$] (X = Cl, Br, or I). *Dalton Trans*. **2013**, *42*, 7224-7232.

3 Mikhailov, M. A.; Brylev, K. A.; Abramov, P. A.; Sakuda, E.; Akagi, S.; Ito, A.; Kitamura, N.; Sokolov, M. N. Synthetic Tuning of Redox, Spectroscopic, and Photophysical Properties of {Mo$_6$I$_8$}$^{4+}$ Core Cluster Complexes by Terminal Carboxylate Ligands. *Inorg. Chem*. **2016**, *55*, 8437-8445.

4 Akagi, S.; Fujii, S.; Horiguchi, T.; Kitamura, N. pKa(L) Dependences of Structural, Electrochemical, and Photophysical Properties of Octahedral Hexamolybdenum(II) Clusters: [Mo$_6$X$_8$L$_6$]$^{2-}$ (X = Br or I; L = Carboxylate). *J. Cluster Sci*. **2017**, *28*, 757-772.

5 Kirakci, K.; Zelenka, J.; Rumlová, M.; Martinčík, J.; Nikl, M.; Ruml, T.; Lang, K. Octahedral Molybdenum Clusters as Radiosensitizers for X-ray Induced Photodynamic Therapy. *J. Mater. Chem. B* **2018**, *6*, 4301-4307.

6 Barras, A.; Cordier, S.; Boukherroub, R. Fast Photocatalytic Degradation of Rhodamine B over [Mo$_6$Br$_8$(N$_3$)$_6$]$^{2-}$ Cluster Units Under Sun Light Irradiation. *Appl. Catal. B* **2012**, *123*, 1-8.

7 Svezhentseva, E. V.; Solovieva, A. O.; Vorotnikov, Y. A.; Kurskaya, O. G.; Brylev, K. A.; Tsygankova, A. R.; Edeleva, M. V.; Gyrylova, S. N.; Kitamura, N.; Efremova, O. A.; Shestopalov, M. A.; Mironov, Y. V.; Shestopalov, A. M. Water-Soluble Hybrid Materials Based on {Mo$_6$X$_8$}$^{4+}$ (X = Cl, Br, I) Cluster Complexes and Sodium Polystyrene Sulfonate. *New J. Chem*. **2017,** *41*, 1670-1676.

8 Cheplakova, A. M.; Solovieva, A. O.; Pozmogova, T. N.; Vorotnikov, Y. A.; Brylev, K. A.; Vorotnikova, N. A.; Vorontsova, E. V.; Mironov, Y. V.; Poveshchenko, A. F.; Kovalenko, K. A.; Shestopalov, M. A. Nanosized Mesoporous Metal-Organic Framework MIL-101 as a Nanocarrier for Photoactive Hexamolybdenum Cluster Compounds. *J. Inorg. Biochem*. **2017**, *166*, 100-107.

9 Solovieva, A. O.; Vorotnikov, Y. A.; Trifonova, K. E.; Efremova, O. A.; Krasilnikova, A. A.; Brylev, K. A.; Vorontsova, E. V.; Avrorov, P. A.; Shestopalova, L. V.; Poveshchenko, A. F.; Mironov, Y. V.; Shestopalov, M. A. Cellular Internalisation, Bioimaging and Dark and Photodynamic Cytotoxicity of Silica Nanoparticles Doped by $\{Mo_6I_8\}^{4+}$ Metal Clusters. *J. Mater. Chem. B* **2016,** *4*, 4839-4846.

10 Brandhonneur, N.; Hatahet, T.; Amela-Cortes, M.; Molard, Y.; Cordier, S.; Dollo, G. Molybdenum cluster loaded PLGA nanoparticles: An Innovative Theranostic Approach for the Treatment of Ovarian Cancer. *Eur. J. Pharm. Biopharm*. **2018**, *125*, 95-105.

11 Dollo, G.; Boucaud, Y.; Amela-Cortes, M.; Molard, Y.; Cordier, S.; Brandhonneur, N. PLGA Nanoparticles Embedding Molybdenum Cluster Salts: Influence of Chemical Composition on Physico-Chemical Properties, Encapsulation Efficiencies, Colloidal Stabilities and In Vitro Release. *Int. J. Pharm.* **2020**, *576*, article no 119025.

12 Kirakci, K.; Demel, J.; Hynek, J.; Zelenka, J.; Rumlová, M.; Ruml, T.; Lang. K. Phosphinate Apical Ligands − A Route to Water-Stable Octahedral Molybdenum Cluster Complex. *Inorg. Chem.* **2019**, *58*, 16546-16552.

13 Beltrán, A.; Mikhailov, M.; Sokolov, M. N.; Pérez-Laguna, V.; Rezusta, A.; Revillo, M. J.; Galindo, F. A Photobleaching Resistant Polymer Supported Hexanuclear Molybdenum Iodide Cluster for Photocatalytic Oxygenations and Photodynamic Inactivation of *Staphylococcus Aureus*. *J. Mater. Chem. B* **2016**, *4*, 5975-5979.

14 Felip-León, C.; Arnau del Valle, C.; Pérez-Laguna, V.; Millán-Lou, M. I.; Miravet, J. F.; Mikhailov, M.; Sokolov, M. N.; Rezusta-López, A.; Galindo, F. Superior Performance of Macroporous over Gel Type Polystyrene as a Support for the Development of Photo-Bactericidal Materials. *J. Mater. Chem. B* **2017**, *5*, 6058-6064.

15 Vorotnikova, N. A.; Alekseev, A. Y.; Vorotnikov, Y. A.; Evtushoka, D. V., Molard, Y.; Amela-Cortes, M.; Cordier, S.; Smolentsev, A. I., Burton, C. G.; Kozhin, P. M.; Zhug, P.; Topham, P. D.; Mironov, Y. V., Bradley, M.; Efremova, O. A.; Shestopalov, M. Octahedral Molybdenum Cluster as a Photoactive Antimicrobial Additive to a fluoroplastic. *Mater. Sci. Eng. C* **2019**, *105*, article no 110150.

16 Kirakci, K.; Zelenka, J.; Rumlová, M.; Cvačka, J.; Ruml, T.; Lang, K. Cationic Octahedral Molybdenum Cluster Complexes Functionalized with Mitochondria-Targeting Ligands: Photodynamic Anticancer and Antibacterial Activities. *Biomater. Sci.* **2019**, *7*, 1386-1392.

17 Hummel, T.; Dutczak, D.; Alekseev, A.Y.; Adamenko, L.S.; Shestopalov, M.A.; Mironov, Y.V.; Enseling, D.; Jüstel, T.; Meyer, H.-J. Photodynamic Properties of Tungsten Iodide Clusters, Incorporated into Silicone: $A_2[M_6I_8L_6]$@Silicone. *RSC Adv.*, **2020**, *10*, 22257-22263.

18 Hall, C. W.; Mah, T. - F. Molecular Mechanisms of Biofilm-Based Antibiotic Resistance and Tolerance in Pathogenic Bacteria. *FEMS Microbiol. Rev.* **2017**, *41*, 276-301.

19 Nguyen, T. K. N.; Grasset, F.; Dierre, B.; Matsunaga, C.; Cordier, S.; Lemoine, P.; Ohashi, N.; Uchikoshi, T. Fabrication of Transparent Thin Film of Octahedral Molybdenum Metal Clusters by Electrophoretic Deposition. *ECS J. Solid State Sci. Tech.* **2016**, *5*, 178-186.

20 Nguyen, T. K. N.; Dierre, B.; Grasset, F.; Renaud, A.; Cordier, S.; Lemoine, P.; Ohashi, N.; Uchikoshi, T. Formation Mechanism of Transparent Mo_6 Metal Atom Cluster Film Prepared by Electrophoretic Deposition. *J. Electrochem. Soc.* **2017**,*164* , 412-418.

21 Nguyen, T. K. N.; Renaud, A.; Dierre, B.; Bouteille, B.; Wilmet, M.; Dubernet, M.; Ohashi, N.; Grasset, F.; Uchikoshi, T. Extended Study on Electrophoretic Deposition Process of Inorganic Octahedral Metal Clusters: Advanced Multifunctional Transparent Nanocomposite Thin Films. *Bull. Chem. Soc. Jpn*. **2018**, *91*, 1763-1774.

22 Nguyen, T. K. N.; Renaud, A.; Wilmet, M.; Dumait, N.; Paofai, S.; Dierre, B.; Chen, W.; Ohashi, N.; Cordier, S.; Grasset, F.; Uchikoshi, T. New Ultra-Violet and Near-Infrared Blocking Filters for Energy Saving Applications: Fabrication of Tantalum Metal Atom Cluster-Based Nanocomposite Thin Films by Electrophoretic Deposition. *J. Mater. Chem. C* **2017**, *5*, 10477-10484.

23 Chen, W.; Nguyen, T. K. N.; Wilmet, M.; Dumait, N.; Makrygenni, O.; Matsui, Y.; Takei, T.; Cordier, S.; Ohashi, N.; Uchikoshi T.; Grasset, F. $ITO@SiO_2$ and $ITO@\{M_6Br_{12}\}@SiO_2$ (M = Nb, Ta) Nanocomposite Films for Ultraviolet-Near Infrared Shielding. *Nanoscale Adv.* **2019**, *1*, 3693-3698.

24 Nguyen, N. T. K.; Dubernet, M.; Matsui, Y.; Wilmet, M.; Shirahata, N.; Rydzek, G.; Dumait, N.; Amela-Cortes, M.; Renaud, A.; Cordier, S.; Molard, Y.; Grasset F.; Uchikoshi, T. Transparent Functional Nanocomposite Films Based on Octahedral Metal Clusters: Synthesis by Electrophoretic Deposition Process and Characterization. *R. Soc. Open Sci.* **2019**, *6*, article no 181647.

25 Renaud, A.; Nguyen, T. K. N.; Grasset, F.; Raissi, M.; Guillon, V.; Delabrouille, F.; Dumait, N.; Jouan, P.-Y.; Cario, L.; Jobic, S.; Pellegrin, Y.; Odobel, F.; Cordier, S.; Uchikoshi, T.; Preparation by Electrophoretic Deposition of Molybdenum Iodide Cluster-Based Functional Nanostructured Photoelectrodes for Solar Cells. *Electrochim. Acta* **2019**, *317*, 737-745.

26 Kirakci, K.; Kubát, P.; Dušek, M.; Fejfarová, K.; Šícha, V.; Mosinger, J.; Lang K. A Highly Luminescent Hexanuclear Molybdenum Cluster: A Promising Candidate toward Photoactive Materials. *Eur. J. Inorg. Chem*. **2012**, 3107-3111.

27 Lang, K.; Mosinger, J.; Wagnerová D. M. Photophysical Properties of Porphyrinoid Sensitizers Non-Covalently Bound to Host Molecules; Models for Photodynamic Therapy. *Coord. Chem. Rev*. **2004**, *248*, 321-350.

28 Dickson, J. S.; Koohmaraie M. Cell Surface Charge Characteristics and their Relationship to Bacterial Attachment to Meat Surfaces. *Appl. Environ. Microbiol*. **1989**, *55*, 832-836.

29 Maruzani, R.; Sutton, G.; Nocerino, P.; Marvasi, M. Exopolymeric Substances (EPS) from Salmonella Enterica: Polymers, Proteins and their Interactions with Plants and Abiotic Surfaces. *J. Microbiol.* **2019**, *57*, 1-8.

30 Wolfmeier, H.; Pletzer, D.; Mansour, S. C.; Hancock, R. E. W. New Perspectives in Biofilm Eradication. *ACS Infectious Diseases* **2018,** *4*, 93-106.

31 Verderosa, A. D.; Totsika, M.; Fairfull-Smith, K. E. Bacterial Biofilm Eradication Agents: A Current Review. *Front Chem* **2019,** *7*, 824-824.

32 Li, J.; Liu, X.; Tan, L.; Cui, Z.; Yang, X.; Liang, Y.; Li, Z.; Zhu, S.; Zheng, Y.; Yeung, K. W. K.; Wang, X.; Wu, S. Zinc-Doped Prussian Blue Enhances Photothermal Clearance of Staphylococcus Aureus and Promotes Tissue Repair in Infected Wounds. *Nat. Commun.* **2019,** *10*, article no 4490.

33 Li, J.; Wu, N. Semiconductor-Based Photocatalysts and Photoelectrochemical Cells for Solar Fuel Generation: A Review. *Catal. Sci. Technol.* **2015,** *5*, 1360-1384.

34 Xie, X.; Mao, C.; Liu, X.; Tan, L.; Cui, Z.; Yang, X.; Zhu, S.; Li, Z.; Yuan, X.; Zheng, Y.; Yeung, K. W. K.; Chu, P. K.; Wu, S. Tuning the Bandgap of Photo-Sensitive Polydopamine/Ag_3PO_4/Graphene Oxide Coating for Rapid, Noninvasive Disinfection of Implants. *ACS Central Sci.* **2018,** *4*, 724-738.

35 Bakhshandeh, S.; Yavari, S. A. Electrophoretic Deposition: A Versatile Tool against Biomaterial Associated Infections, *J. Mater. Chem. B* **2018**, *6*, 1128-1148.

Table of Contents